molecular pharmaceutics

Article

pubs.acs.org/molecularpharmaceutics

Design, Synthesis, and Validation of Axl-Targeted Monoclonal Antibody Probe for microPET Imaging in Human Lung Cancer Xenograft

Shuanglong Liu,[†,#] Dan Li,[†,‡,#] Jiacong Guo,[†,§,#] Nicolette Canale,[†] Xiuqing Li,[∥] Ren Liu,[∥] Valery Krasnoperov,[⊥] Parkash S. Gill,[∥] Peter S. Conti,[†] Hong Shan,*[,‡] and Zibo Li*[,†]

[†]Molecular Imaging Center, Department of Radiology, University of Southern California, Los Angeles, California 90089, United States

[‡]Department of Radiology, The Third Affiliated Hospital of Sun Yat-sen University, Guangzhou 510630, China

[§]Department of Molecular Microbiology & Immunology, University of Southern California, Los Angeles, California 90089, United States

[∥]Department of Pathology, University of Southern California, Los Angeles, California 90089, United States

[⊥]Vasgene Therapeutics, Inc., Los Angeles, California 90033, United States

ABSTRACT: Accumulating experimental evidence indicates that overexpression of the oncogenic receptor tyrosine kinase, Axl, plays a key role in the tumorigenesis and metastasis of various types of cancer. The objective of this study is to design a novel imaging probe based on the monoclonal antibody, h173, for microPET imaging of Axl expression in human lung cancer. A bifunctional chelator, DOTA, was conjugated to h173, followed by radiolabeling with ^{64}Cu. The binding of DOTA-h173 to the Axl receptor was first evaluated by a cell uptake assay and flow cytometry analysis using human lung cancer cell lines. The probe ^{64}Cu-DOTA-h173 was further evaluated by microPET imaging, and *ex vivo* histology studies in the Axl-positive A549 tumors. *In vitro* cellular study showed that Axl probe, ^{64}Cu-DOTA-h173, was highly immuno-reactive with A549 cells. Western blot analysis confirmed that Axl is highly expressed in the A549 cell line. For microPET imaging, the A549 xenografts demonstrated a significantly higher ^{64}Cu-DOTA-h173 uptake compared to the NCI-H249 xenograft (a negative control model). Furthermore, ^{64}Cu-DOTA-h173 uptake in A549 is significantly higher than that of ^{64}Cu-DOTA-hIgG. Immuno-fluorescence staining was consistent with the *in vivo* micro-PET imaging results. In conclusion, ^{64}Cu-DOTA-h173 could be potentially used as a probe for noninvasive imaging of Axl expression, which could collect important information regarding tumor response to Axl-targeted therapeutic interventions.

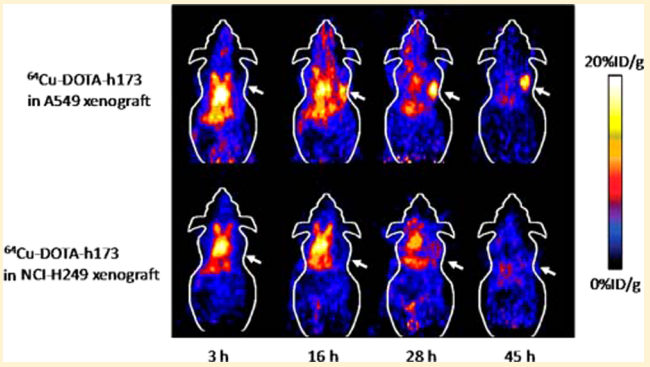

KEYWORDS: *Axl receptor, monoclonal antibody, positron emission tomography (PET), lung cancer*

INTRODUCTION

Receptor tyrosine kinases (RTKs) are a class of protein kinases that play a critical role in the development and progression of various types of cancer. Recently, approximately 20 different RTK classes have been identified, with Axl belonging to one of these classes.[1,2] The Axl receptor tyrosine kinase was isolated as a transforming gene from primary human myeloid leukemia cells.[3] Axl is implicated in vascular remodeling, regulation of smooth muscle cells, and migration of endothelial cells.[4−6] In recent years, the significant role of Axl in tumor initiation and metastases has been reinforced by the fact that Axl is overexpressed in multiple cancer types including prostate,[7] breast,[8−10] lung,[11−15] gastric,[16] glioblastoma,[17,18] and Kaposi sarcoma.[19] Several studies also indicate that the expression level of Axl is highly correlated with lung tumor progression[15] and invasiveness of breast cancer cells.[10] In addition, Axl is identified as a potential therapeutic target for overcoming EGFR inhibitor resistance[11] and for lapatinib and trastuzumab resistance in breast cancer cells.[8]

In order to hasten the pace of developing anti-Axl based cancer therapy for clinical trials, it is desirable to establish effective methods to quantify Axl expression *in vivo*. Molecular imaging techniques have been widely used for diagnosis and therapy management through evaluation of molecular marker and receptor expression *in vivo*. In particular, positron emission tomography (PET) has gained a remarkable amount of

Special Issue: Positron Emission Tomography: State of the Art

Received: April 25, 2014
Revised: June 24, 2014
Accepted: June 30, 2014
Published: June 30, 2014

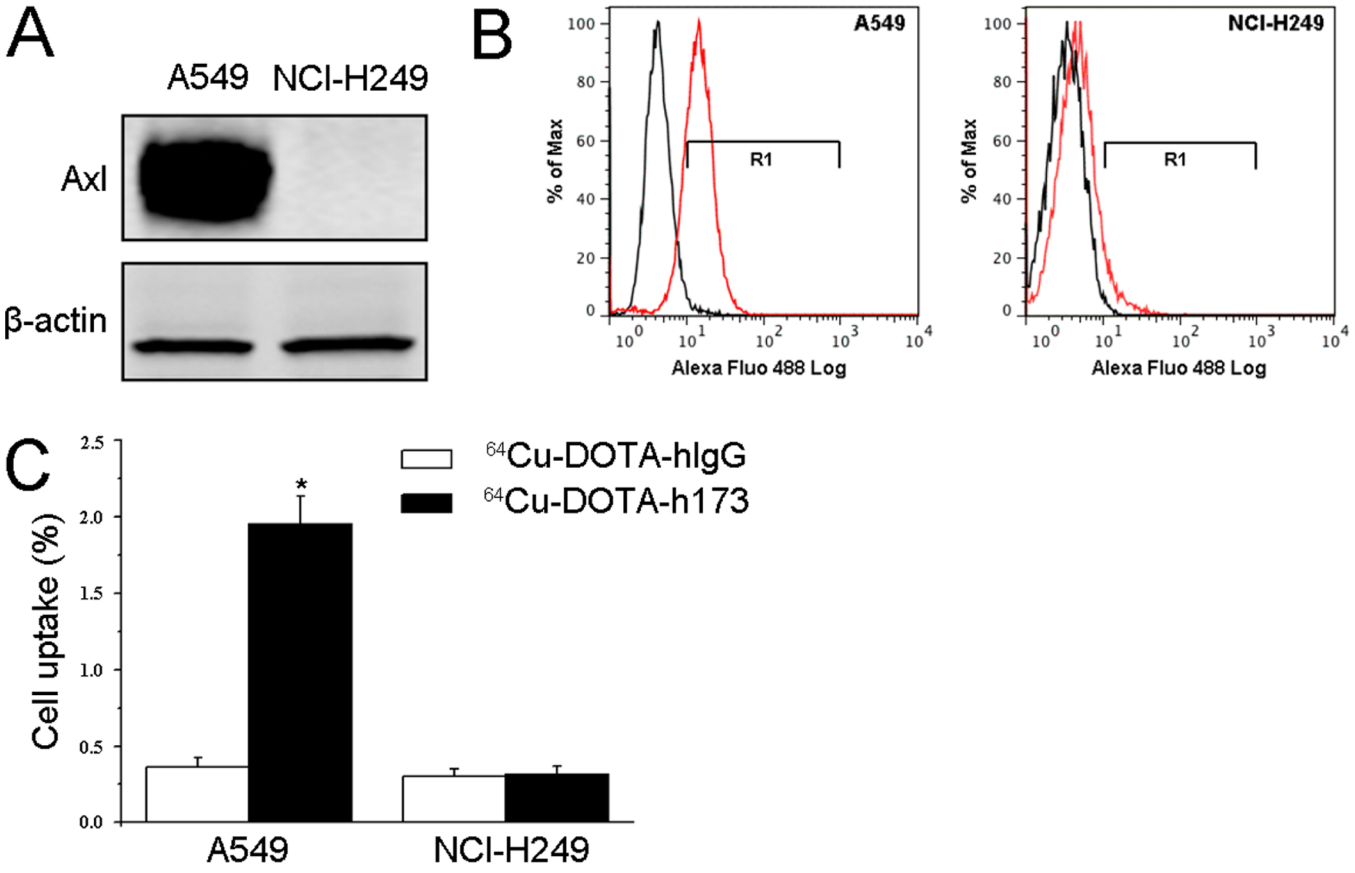

Figure 1. (A) Western blot of Axl in A549 and NCl-H249 tumor cells. (B) FACS analysis of A549 and NCl-H249 tumor cells using h173 as the primary antibody. (C) Cell uptake assay of ^{64}Cu-DOTA-hIgG and ^{64}Cu-DOTA-h173 on A549 and NCl-H249 tumor cells (n = 3, mean ± SD).

attention due to its quantitative imaging properties and high sensitivity. In fact, there is a considerable amount of interest in development of imaging probes for PET that can serve as companion diagnostics for novel therapeutics. However, to the best of our knowledge, no PET probe targeting Axl has been reported in previous literature.

Recently, monoclonal antibodies of murine origin that are specific for Axl have been developed. One of these antibodies, m173, appears to bind to the first fibronection domain.[19] To enhance clinical application, humanized 173 (h173) was also produced as reported.[20] Because of the strong and specific binding of h173 to Axl, we hypothesized that radiolabeled h173 could depict the Axl receptor distribution *in vivo* by PET. The data obtaining by PET imaging could be used to confirm the presence of Axl, which would be important clinical information in determining the utility of Axl-targeted chemo- and radiotherapy in receptor positive patients. In this study, we radiolabeled h173 with ^{64}Cu to create an antibody based PET probe to noninvasively quantify Axl expression *in vivo*.

MATERIALS AND METHODS

Cell Culture and Fluorescence-Activated Cell Sorting (FACS) Analysis. Human small cell lung cancer A549 cell line and nonsmall cell lung cancer cell line NCI-H249, obtained from American Type Culture Collection (Manassas, VA), were grown in RPMI-1640 supplemented with 10% fetal bovine serum. For FACS analysis, adherently grown A549 cells were detached by applying nonenzymatical citric saline buffer.[21] NCI-H249 cells were grown in suspension. To minimize nonspecific uptake, the procedures were performed on ice. Aliquots of cells were blocked with 10% normal goat serum, incubated with anti-Axl primary antibody h173 (kindly provided by Vasgene Therapeutics Inc., Los Angeles, CA) produced using composite human antibody technology[20] and goat antihuman Alexa Fluor 488 (Invitrogen, Paisley, Scotland) in sequence. Subsequently, cells were measured by flow cytometry (CyAn analyzer, Beckman Coulter). Cells without the incubation of primary antibody were used as negative controls.

Western Blot. A Western blot was performed as described previously.[22,23] Proteins extracted from A549 and NCI-H249 tumor cells were fractionated using 4−20% SDS-PAGE (Bio-Rad). After protein transfer, polyvinylidene difluoride membrane was blocked with 5% nonfat dry milk, probed with anti-Axl primary antibody (Cat #8661, Cell Signaling Technology, Beverly, MA) and secondary antibody, and developed. β-actin was used as an internal control.

Chemistry and Radiochemistry. h173 was conjugated with DOTA-NHS synthesized *in situ* (molar ratio, 1:20) through amino groups to form DOTA-h173. The synthesis followed literature reported procedures.[23] Negative control antibody, human normal immunoglobulin G (hIgG), was purchased from Rockland (Gilbertsville, PA). Control probe DOTA-hIgG was also synthesized using the same procedure. After ^{64}Cu (purchased from Washington University, St. Louis) labeling,[23] probes were used for further *in vitro* and *in vivo* experiments.

Binding Activity Assay. Axl binding activity of DOTA-h173 and DOTA-hIgG was performed through a bead-based binding assay with Axl-alkaline phosphatase (AP) (kindly

dx.doi.org/10.1021/mp500307t | *Mol. Pharmaceutics* 2014, 11, 3974−3979

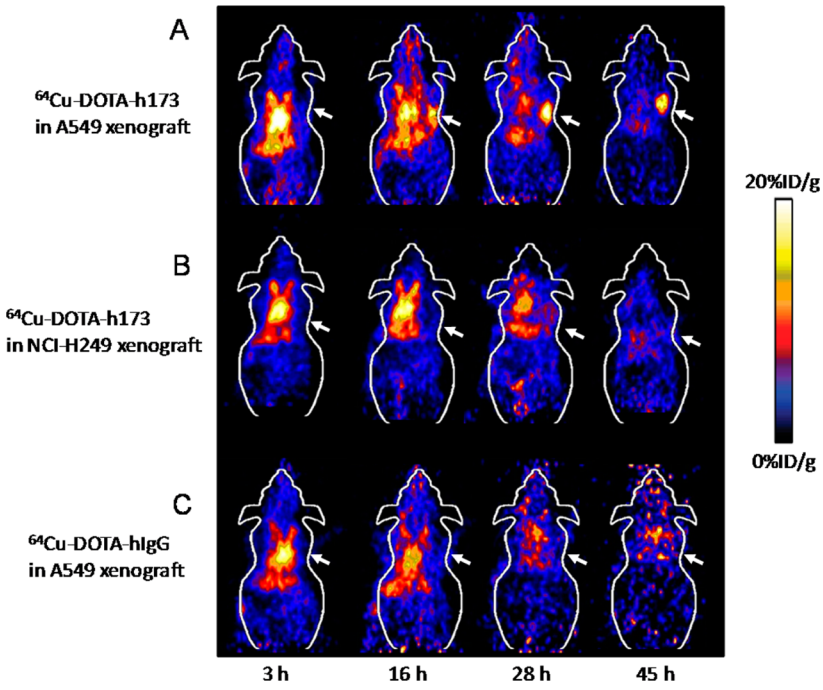

Figure 2. Decay-corrected whole-body coronal microPET images from a static scan at 3, 16, 28, and 45 h p.i. of (A) ^{64}Cu-DOTA-h173 into A549 tumor bearing mice, (B) ^{64}Cu-DOTA-h173 into NCl-H249 tumor bearing mice, and (C) ^{64}Cu-DOTA-hIgG into A549 tumor bearing mice. Arrows indicate tumors.

provided by Vasgene Therapeutics Inc., Los Angeles, CA) as reported previously.[22,23] Each sample was repeated in triplicate.

Cell Uptake Assay. Cell uptake of probes in A549 and NCI-H249 tumor cells was performed as described previously.[24] Adherently grown A549 cells were harvested by applying nonenzymatical citric saline buffer.[21] NCI-H249 cells were grown in suspension. 5×10^5 cells were suspended in 200 μL of complete cell culture media, and 37 kBq of ^{64}Cu-DOTA-h173 and ^{64}Cu-DOTA-hIgG was added. After 1.5 h of incubation, unbound probes were removed by washing twice with cold PBS. Finally, cells were sedimented by centrifugation, and the radioactivity in each cell pellet was counted. The data were obtained in triplicate.

Tumor Xenografts and microPET Imaging. All animal experiments were performed under a protocol approved by the University of Southern California Institutional Animal Care and Use Committee (IACUC). To establish a lung tumor xenograft model, 2×10^6 of A549 or NCI-H249 cells were subcutaneously injected in the right shoulder of nude mice as previous reported.[22,23]

The tumor-bearing mice were injected with 3.7−7.4 MBq of ^{64}Cu probes via tail veins. For each probe, 3 randomly selected mice were used. Multiple static scans were obtained at 3, 16, 28, and 45 h postinjection (p.i.). PET imaging and analysis were conducted by using a Siemens microPET R4 rodent model scanner as described previously.[23,25]

Immunofluorescence Staining. Antibody distribution was evaluated through immunofluorescence staining as previously reported.[23] Tumors were dissected at 48 h p.i. of 30 μg of DOTA-h173 or DOTA-hIgG. Antibody distribution was localized by using secondary antibody goat antihuman Alexa Fluor 568 (Invitrogen, Paisley, Scotland).

Statistical Analysis. All of the quantitative data are given as means ± SD of three independent measurements. Student's *t*-test was used to analyze the data. Statistical significance was assigned for P values < 0.05.

RESULTS

Chemistry, Radiochemistry, and Binding Activity Assay. h173 and hIgG were conjugated with ^{64}Cu chelator DOTA through amino groups, which lead to DOTA-h173 and DOTA-hIgG. After ^{64}Cu labeling, the radiochemical yields for ^{64}Cu-DOTA-h173 and ^{64}Cu-DOTA-hIgG were 44.5% and 57.6%, respectively. The specific activity of ^{64}Cu-DOTA-h173 and ^{64}Cu-DOTA-hIgG was estimated to be 1.48−2.96 GBq/mg antibody. To investigate the influence of DOTA conjugation on Axl binding ability, a binding activity assay was conducted. Axl binding activity was preserved with DOTA-h173 (98.27% ± 1.29%). On the contrary, DOTA-hIgG showed 0.015 ± 0.003% binding activity toward this target.

Axl Expression Assay on Cell Lines and Cell Uptake Study. We used A549 and NCI-H249 human lung cancer cell lines for this study. A Western blot was performed to detect Axl expression in these two cell lines. As shown in Figure 1A, A549 overexpressed Axl, while NCI-H249 was negative. Fluorescence-activated Cell Sorting (FACS) data demonstrated that the percentage of Axl positive in A549 and NCI-H249 was 84.40 ± 1.56% and 2.43 ± 0.27%, respectively (Figure 1B). Cell uptake study was also conducted (Figure 1C). In A549 cells, the cell uptake of ^{64}Cu-DOTA-h173 (1.96 ± 0.10%) was significantly higher than ^{64}Cu-DOTA-hIgG (0.36 ± 0.04%) (P < 0.05). The cell uptake of both ^{64}Cu-DOTA-h173 (0.32 ± 0.05%) and ^{64}Cu-DOTA-hIgG (0.30 ± 0.05%) in NCI-H249 cells was low and showed no significant difference between them (P > 0.05). The above *in vitro* data demonstrated that ^{64}Cu-DOTA-h173 probe was Axl-specific.

***In Vivo* MicroPET Imaging Study.** The *in vivo* microPET imaging study was performed on both A549 and NCI-H249 tumor xenograft mice after the injection of ^{64}Cu-DOTA-h173

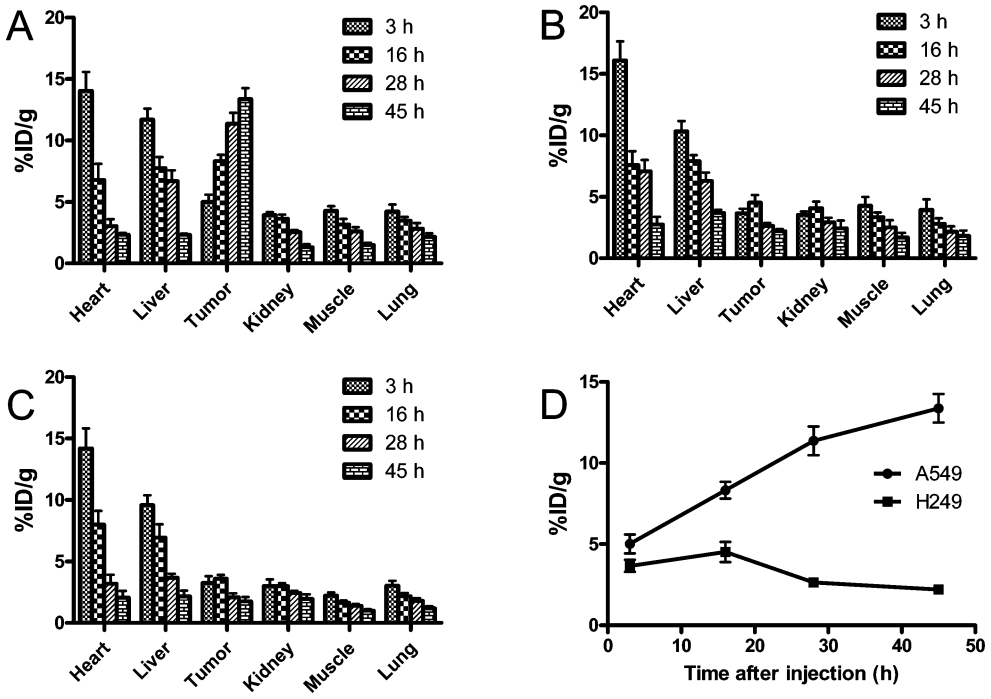

Figure 3. Major organ radioactivity accumulation quantification from a static scan at 3, 16, 28, and 45 h p.i. of (A) ^{64}Cu-DOTA-h173 into A549 tumor bearing mice, (B) ^{64}Cu-DOTA-h173 into NCl-H249 tumor bearing mice, and (C) ^{64}Cu-DOTA-hIgG into A549 tumor bearing mice. (D) Time course of A549 and NCl-H249 tumor uptake of ^{64}Cu-DOTA-h173 from 3 to 45 h p.i.

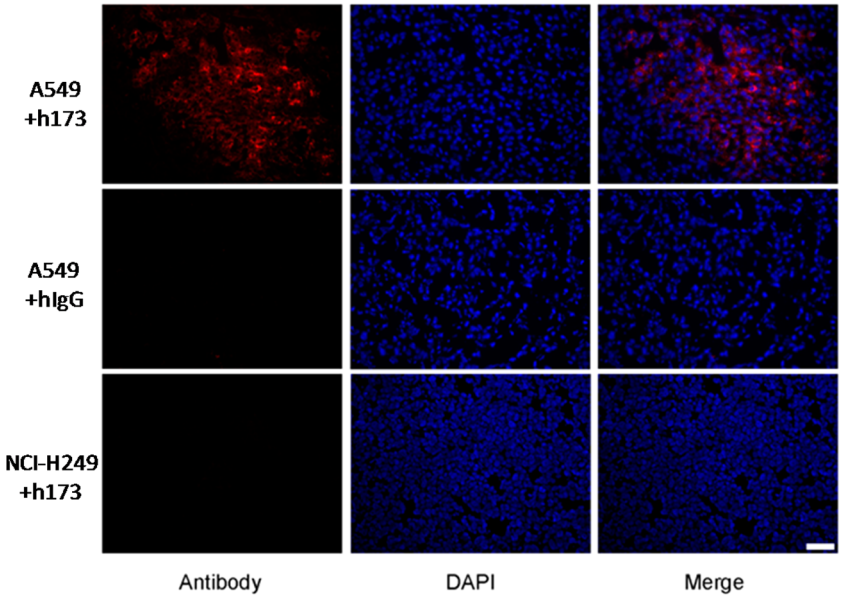

Figure 4. Immunofluorescence staining of antibodies in A549 and NCl-H249 tumor sections. Scale bar, 20 μm.

or ^{64}Cu-DOTA-hIgG. Representative decay-corrected coronal images are shown in Figure 2. At an early time point, both ^{64}Cu-DOTA-h173 and ^{64}Cu-DOTA-hIgG demonstrated high heart uptake because of the relative long circulation half-life of antibodies *in vivo*. Similarly, the liver also had relatively high uptake, which could be attributed to the nonspecific uptake of tracers through the reticular-endothelial system. As for other organs, such as the lung, their uptake was not significantly different from the background such as muscle. The uptake in the tumor or other organs was calculated from the ROI analysis and shown in Figure 3. The A549 tumor uptake of ^{64}Cu-DOTA-h173 was 5.02 ± 1.00, 8.32 ± 0.89, 11.37 ± 1.53, and 13.37 ± 1.53 %ID/g (percentage of injected dose per gram of tissue) at 3, 16, 28, and 45 h p.i., respectively. The NCI-H249 tumor uptake of ^{64}Cu-DOTA-h173 was 3.66 ± 0.64, 4.52 ± 1.08, 2.65 ± 0.36, and 2.21 ± 0.30 %ID/g at 3, 16, 28, and 45 h p.i., respectively. ^{64}Cu-DOTA-h173 uptake in A549 tumors was significantly higher than in NCI-H249 tumors ($P < 0.05$, Figure 3D) at 16, 28, and 45 h time points. The A549-tumor to lung ratios were 1.21 ± 0.25, 2.42 ± 0.36, 4.35 ± 1.80, and 6.53 ± 2.10 %ID/g at 3, 16, 28, and 45 h p.i. of ^{64}Cu-DOTA-h173, respectively. ^{64}Cu-DOTA-hIgG was also imaged in A549 tumor models to validate the target specificity of ^{64}Cu-DOTA-h173. The A549 tumor uptake of ^{64}Cu-DOTA-hIgG at all time points

dx.doi.org/10.1021/mp500307t | *Mol. Pharmaceutics* 2014, 11, 3974−3979

examined was comparatively low (3.26 ± 0.94, 3.59 ± 0.54, 2.09 ± 0.55, and 1.76 ± 0.58 %ID/g at 3, 16, 28, and 45 h p.i., respectively), which is similar to the muscle uptake (4.28 ± 1.23, 3.35 ± 0.65, 2.52 ± 0.98, and 1.69 ± 0.66 %ID/g at 3, 16, 28, and 45 h p.i., respectively).

Probe Distribution Analysis in Tumor Tissues. Probe distribution analysis in tumor tissues was conducted through immunofluorescence staining. As shown in Figure 4, more h173 accumulated in Axl-positive A549 tumors than hIgG control. In Axl-negative NCI-H249 tumors, there was minimal accumulation of h173. Therefore, both *in vitro* and *in vivo* data indicated that ^{64}Cu-DOTA-h173 could be applied for noninvasive imaging of Axl expression.

DISCUSSION

Up until now, 20 distinct subfamilies of RTKs have been found and categorized according to their identities in their amino acid sequence and structural similarities in their extracellular regions. One of these, the subfamily TAM, is composed of Axl, Sky, and Mer. Axl and its ligand, Gas6, have been found to play a pivotal role in the survival and metastasis of multiple cancers and other diseases.[7,16,26−30]

In this study, the novel ^{64}Cu-labeled h173 antibody was synthesized and characterized to demonstrate that imaging Axl expression with PET is possible. Attachment of ^{64}Cu to a targeting molecule required the use of a bifunctional chelator (BFC). In our experiment, the chelator used was commercially available DOTA. Binding activity assay showed that DOTA-h173 preserved 98.27% ± 1.29% Axl binding activity. FACS (Figure 1B) and the cell uptake study (Figure 1C) further confirmed that h173 could bind to Axl-positive A549 lung cancer cells, but not to Axl-negative NCI-H249 tumors, indicating that h173 antibody was Axl-specific. Western detects both cell surface and cytoplasm Axl while flow cytometry detects only cell surface Axl. Therefore, the receptor expression difference in flow cytometry was not as drastic as the western data.

The *in vivo* microPET imaging study was performed on both A549 and NCI-H249 tumor xenograft mice (Figures 2 and 3). ^{64}Cu-DOTA-h173 uptake in A549 tumors increased with time, and a better tumor-to-background contrast was displayed at late time points (28 h, 45 h p.i.). Both active uptake (contributed by h173-Axl interaction) and passive uptake (contributed by the enhanced permeability and retention effect) lead to ^{64}Cu-DOTA-h173 accumulation in A549 tumors. In contrast, tumor accumulation of ^{64}Cu-DOTA-hIgG was only caused by passive uptake. The A549 tumor uptake of ^{64}Cu-DOTA-hIgG at all time points examined was comparatively low. Thus, the target specificity of ^{64}Cu-DOTA-h173 was confirmed. On the contrary, ^{64}Cu-DOTA-h173 uptake in NCI-H249 tumors was significantly lower than in A549 tumors ($P < 0.05$, Figure 3D). As h173 only recognizes human Axl, it does not target murine vasculature, which also expresses Axl in tumor xenograft mouse models, according to the published studies.[31,32] Therefore, the difference in tumor uptake should reflect the Axl expression levels of different lung tumor cells. We would like to point out that tumors without Axl expression could still show some tracer uptake due to the presence of nonspecific accumulation. In order to accurately reflect Axl receptor expression level with immunoPET, the contribution from "passive" targeting needs to be considered during data analysis. However, in humans, use of ^{64}Cu-DOTA-h173 for Axl-targeted imaging might provide higher contrast from surrounding tissues due to the fact that it recognizes both tumor cells and associated vasculature. In addition, highly selective localization of h173 to the tumor bed could lead to applications with therapeutic radionuclides, such as ^{90}Y, ^{177}Lu, or ^{213}Bi for targeted radiation therapy.[33]

CONCLUSIONS

We have developed a receptor-targeted PET probe for detection of Axl-positive tumors. This study shows that ^{64}Cu-DOTA-h173, based on a humanized Axl-specific monoclonal antibody, displays high target specificity both *in vitro* and *in vivo*. The positive correlation between Axl expression levels and tumor invasiveness in multiple cancer types makes ^{64}Cu-DOTA-h173 potentially clinically useful for staging Axl-positive cancers and managing patients with Axl-targeted therapy.

AUTHOR INFORMATION

Corresponding Authors

*(H.S.) E-mail: shanhong@mail.sysu.edu.cn.

*(Z.L.) E-mail: ziboli@email.unc.edu.

Author Contributions

#S.L., D.L., and J.G. contributed equally to this work.

Notes

The authors declare no competing financial interest.

ACKNOWLEDGMENTS

This work was supported by the NIBIB (R21 1 r21 eb012294-01a1 and 1R01EB014354-01A1), Early (Margaret E.) Medical Research Trust, the American Cancer Society (121991-MRSG-12-034-01-CCE), SC CTSI (12-2176-3135), Department of Defense (BC102678), Vasgene Therapeutics Inc. (NIH: CA168158-01 and CA171538-01), National Natural Science Foundation of China (No. U1032002, 81071206, 81271621, and 81301266), and Key Clinical Research Project of Public Health Ministry of China 2010-2012 (No. 164).

REFERENCES

(1) Hafizi, S.; Dahlback, B. Signalling and functional diversity within the Axl subfamily of receptor tyrosine kinases. *Cytokine Growth Factor Rev.* **2006**, *17*, 295−304.

(2) Hafizi, S.; Dahlback, B. Gas6 and protein S. Vitamin K-dependent ligands for the Axl receptor tyrosine kinase subfamily. *FEBS J.* **2006**, *273*, 5231−5244.

(3) O'Bryan, J. P.; Frye, R. A.; Cogswell, P. C.; Neubauer, A.; Kitch, B.; Prokop, C.; Espinosa, R., 3rd; Le Beau, M. M.; Earp, H. S.; Liu, E. T. Axl, a transforming gene isolated from primary human myeloid leukemia cells, encodes a novel receptor tyrosine kinase. *Mol. Cell. Biol.* **1991**, *11*, 5016−5031.

(4) Melaragno, M. G.; Fridell, Y. W.; Berk, B. C. The Gas6/Axl system: a novel regulator of vascular cell function. *Trends Cardiovasc. Med.* **1999**, *9*, 250−253.

(5) Korshunov, V. A.; Mohan, A. M.; Georger, M. A.; Berk, B. C. Axl, a receptor tyrosine kinase, mediates flow-induced vascular remodeling. *Circ. Res.* **2006**, *98*, 1446−1452.

(6) Collett, G. D.; Sage, A. P.; Kirton, J. P.; Alexander, M. Y.; Gilmore, A. P.; Canfield, A. E. Axl/phosphatidylinositol 3-kinase signaling inhibits mineral deposition by vascular smooth muscle cells. *Circ. Res.* **2007**, *100*, 502−509.

(7) Sainaghi, P. P.; Castello, L.; Bergamasco, L.; Galletti, M.; Bellosta, P.; Avanzi, G. C. Gas6 induces proliferation in prostate carcinoma cell lines expressing the Axl receptor. *J. Cell. Physiol.* **2005**, *204*, 36−44.

(8) Liu, L.; Greger, J.; Shi, H.; Liu, Y.; Greshock, J.; Annan, R.; Halsey, W.; Sathe, G. M.; Martin, A.-M.; Gilmer, T. M. Novel mechanism of lapatinib resistance in HER2-positive breast tumor cells: Activation of AXL. *Cancer Res.* **2009**, *69*, 6871−6878.

(9) Gjerdrum, C.; Tiron, C.; Høiby, T.; Stefansson, I.; Haugen, H.; Sandal, T.; Collett, K.; Li, S.; McCormack, E.; Gjertsen, B. T.; Micklem, D. R.; Akslen, L. A.; Glackin, C.; Lorens, J. B. Axl is an essential epithelial-to-mesenchymal transition-induced regulator of breast cancer metastasis and patient survival. *Proc. Natl. Acad. Sci. U.S.A.* **2010**, *107*, 1124−1129.
(10) Zhang, Y.-X.; Knyazev, P. G.; Cheburkin, Y. V.; Sharma, K.; Knyazev, Y. P.; Őrfi, L.; Szabadkai, I.; Daub, H.; Kéri, G.; Ullrich, A. AXL is a potential target for therapeutic intervention in breast cancer progression. *Cancer Res.* **2008**, *68*, 1905−1915.
(11) Byers, L. A.; Diao, L.; Wang, J.; Saintigny, P.; Girard, L.; Peyton, M.; Shen, L.; Fan, Y.; Giri, U.; Tumula, P. K.; Nilsson, M. B.; Gudikote, J.; Tran, H.; Cardnell, R. J. G.; Bearss, D. J.; Warner, S. L.; Foulks, J. M.; Kanner, S. B.; Gandhi, V.; Krett, N.; Rosen, S. T.; Kim, E. S.; Herbst, R. S.; Blumenschein, G. R.; Lee, J. J.; Lippman, S. M.; Ang, K. K.; Mills, G. B.; Hong, W. K.; Weinstein, J. N.; Wistuba, I. I.; Coombes, K. R.; Minna, J. D.; Heymach, J. V. An epithelial−mesenchymal transition gene signature predicts resistance to EGFR and PI3K inhibitors and identifies axl as a therapeutic target for overcoming EGFR inhibitor resistance. *Clin. Cancer Res.* **2013**, *19*, 279−290.
(12) Postel-Vinay, S.; Ashworth, A. AXL and acquired resistance to EGFR inhibitors. *Nat. Genet.* **2012**, *44*, 835−836.
(13) Vaughan, C. A.; Singh, S.; Windle, B.; Yeudall, W. A.; Frum, R.; Grossman, S. R.; Deb, S. P.; Deb, S. Gain-of-function activity of mutant p53 in lung cancer through up-regulation of receptor protein tyrosine kinase Axl. *Genes Cancer* **2012**, *3*, 491−502.
(14) Ishikawa, M.; Sonobe, M.; Nakayama, E.; Kobayashi, M.; Kikuchi, R.; Kitamura, J.; Imamura, N.; Date, H. Higher expression of receptor tyrosine kinase Axl, and differential expression of its ligand, Gas6, predict poor survival in lung adenocarcinoma patients. *Ann. Surg. Oncol.* **2012**, *Suppl 3*, S467−S476.
(15) Shieh, Y. S.; Lai, C. Y.; Kao, Y. R.; Shiah, S. G.; Chu, Y. W.; Lee, H. S.; Wu, C. W. Expression of axl in lung adenocarcinoma and correlation with tumor progression. *Neoplasia* **2005**, *7*, 1058−1064.
(16) Wu, C. W.; Li, A. F.; Chi, C. W.; Lai, C. H.; Huang, C. L.; Lo, S. S.; Lui, W. Y.; Lin, W. C. Clinical significance of AXL kinase family in gastric cancer. *Anticancer Res.* **2002**, *22*, 1071−1078.
(17) Hutterer, M.; Knyazev, P.; Abate, A.; Reschke, M.; Maier, H.; Stefanova, N.; Knyazeva, T.; Barbieri, V.; Reindl, M.; Muigg, A.; Kostron, H.; Stockhammer, G.; Ullrich, A. Axl and growth arrest-specific gene 6 are frequently overexpressed in human gliomas and predict poor prognosis in patients with glioblastoma multiforme. *Clin. Cancer Res.* **2008**, *14*, 130−138.
(18) Vajkoczy, P.; Knyazev, P.; Kunkel, A.; Capelle, H.-H.; Behrndt, S.; von Tengg-Kobligk, H.; Kiessling, F.; Eichelsbacher, U.; Essig, M.; Read, T.-A.; Erber, R.; Ullrich, A. Dominant-negative inhibition of the Axl receptor tyrosine kinase suppresses brain tumor cell growth and invasion and prolongs survival. *Proc. Natl. Acad. Sci. U.S.A.* **2006**, *103*, 5799−5804.
(19) Liu, R.; Gong, M.; Li, X.; Zhou, Y.; Gao, W.; Tulpule, A.; Chaudhary, P. M.; Jung, J.; Gill, P. S. Induction, regulation, and biologic function of Axl receptor tyrosine kinase in Kaposi sarcoma. *Blood* **2010**, *116*, 297−305.
(20) Krasnoperov, V.; Kumar, S. R.; Ley, E.; Li, X.; Scehnet, J.; Liu, R.; Zozulya, S.; Gill, P. S. Novel EphB4 monoclonal antibodies modulate angiogenesis and inhibit tumor growth. *Am. J. Pathol.* **2010**, *176*, 2029−2038.
(21) Zhang, B.; Shan, H.; Li, D.; Li, Z. R.; Zhu, K. S.; Jiang, Z. B.; Huang, M. S. Different methods of detaching adherent cells significantly affect the detection of TRAIL receptors. *Tumori* **2012**, *98*, 800−803.
(22) Li, D.; Liu, S.; Liu, R.; Park, R.; Hughes, L.; Krasnoperov, V.; Gill, P. S.; Li, Z.; Shan, H.; Conti, P. S. Targeting the EphB4 receptor for cancer diagnosis and therapy monitoring. *Mol. Pharmaceutics* **2013**, *10*, 329−336.
(23) Liu, S.; Li, D.; Park, R.; Liu, R.; Xia, Z.; Guo, J.; Krasnoperov, V.; Gill, P. S.; Li, Z.; Shan, H.; Conti, P. S. PET imaging of colorectal and breast cancer by targeting EphB4 receptor with 64Cu-labeled hAb47 and hAb131 antibodies. *J. Nucl. Med.* **2013**, *54*, 1094−1100.
(24) Liu, S.; Li, D.; Shan, H.; Gabbai, F. P.; Li, Z.; Conti, P. S. Evaluation of (18)F-labeled BODIPY dye as potential PET agents for myocardial perfusion imaging. *Nucl. Med. Biol.* **2014**, *41*, 120−126.
(25) Liu, S.; Li, D.; Huang, C. W.; Yap, L. P.; Park, R.; Shan, H.; Li, Z.; Conti, P. S. Efficient construction of PET/fluorescence probe based on sarcophagine cage: an opportunity to integrate diagnosis with treatment. *Mol. Imaging Biol.* **2012**, *14*, 718−724.
(26) Ammoun, S.; Provenzano, L.; Zhou, L.; Barczyk, M.; Evans, K.; Hilton, D. A.; Hafizi, S.; Hanemann, C. O. Axl/Gas6/NFkappaB signalling in schwannoma pathological proliferation, adhesion and survival. *Oncogene* **2014**, *33*, 336−346.
(27) Ekman, C.; Jönsen, A.; Sturfelt, G.; Bengtsson, A. A.; Dahlbäck, B. Plasma concentrations of Gas6 and sAxl correlate with disease activity in systemic lupus erythematosus. *Rheumatology* **2011**, *50*, 1064−1069.
(28) Gustafsson, A.; Martuszewska, D.; Johansson, M.; Ekman, C.; Hafizi, S.; Ljungberg, B.; Dahlback, B. Differential expression of Axl and Gas6 in renal cell carcinoma reflecting tumor advancement and survival. *Clin. Cancer Res.* **2009**, *15*, 4742−4749.
(29) Gustafsson, A.; Bostrom, A. K.; Ljungberg, B.; Axelson, H.; Dahlback, B. Gas6 and the receptor tyrosine kinase Axl in clear cell renal cell carcinoma. *PLoS One* **2009**, *4*, e7575.
(30) Sun, W.; Fujimoto, J.; Tamaya, T. Coexpression of Gas6/Axl in human ovarian cancers. *Oncology* **2004**, *66*, 450−457.
(31) Hutterer, M.; Knyazev, P.; Abate, A.; Reschke, M.; Maier, H.; Stefanova, N.; Knyazeva, T.; Barbieri, V.; Reindl, M.; Muigg, A.; Kostron, H.; Stockhammer, G.; Ullrich, A. Axl and growth arrest-specific gene 6 are frequently overexpressed in human gliomas and predict poor prognosis in patients with glioblastoma multiforme. *Clin. Cancer Res.* **2008**, *14*, 130−138.
(32) Sensi, M.; Catani, M.; Castellano, G.; Nicolini, G.; Alciato, F.; Tragni, G.; De Santis, G.; Bersani, I.; Avanzi, G.; Tomassetti, A.; Canevari, S.; Anichini, A. Human cutaneous melanomas lacking MITF and melanocyte differentiation antigens express a functional Axl receptor kinase. *J. Invest. Dermatol.* **2011**, *131*, 2448−2457.
(33) Song, H.; Sgouros, G. Radioimmunotherapy of solid tumors: searching for the right target. *Curr. Drug Delivery* **2011**, *8*, 26−44.